International Journal of Pharmaceutics 629 (2022) 122390

Contents lists available at ScienceDirect

International Journal of Pharmaceutics

journal homepage: www.elsevier.com/locate/ijpharm

Glass transition, crystallization kinetics, and inter-conformer relaxation dynamics of amorphous mitotane and related compounds

Michela Romanini [a,b,*], Alex Pérez Valmaseda [a], Roberto Macovez [a,b]

[a] Grup de Caracterització de Materials, Departament de Física, Universitat Politècnica de Catalunya, EEBE, Av. Eduard Maristany 10-14, E-08019 Barcelona, Catalonia, Spain

[b] Barcelona Research Center in Multiscale Science and Engineering, Universitat Politècnica de Catalunya, Campus Diagonal-Besòs, Av. Eduard Maristany 10-14, E-08019 Barcelona, Catalonia, Spain

ARTICLE INFO

Keywords:
Amorphous formulations
Physical stability
Molecular mobility
Inter-conformer conversion
Crystal growth
Dielectric spectroscopy

ABSTRACT

We employ differential scanning calorimetry, broadband dielectric spectroscopy and optical microscopy to investigate the glass transition, molecular relaxation dynamics, and isothermal recrystallization kinetics of amorphous mitotane, the only drug approved for the pharmacological treatment of adrenocortical carcinoma. Amorphous mitotane displays a glass transition at $T_g = 243 \pm 1$ K, characterized by relatively low fragility index of 68 ± 2. Besides the structural and Johari-Goldstein relaxations, amorphous mitotane displays an intramolecular relaxation with activation energy of 25 ± 1 kJ mol^{-1}. The same relaxation process, with virtually the same activation energy and relaxation times, is observed in the closely-related *o,p'*-dichlorobenzophenone compound, which allows identifying it as the rotation of the chlorobenzene ring with the chlorine closest to the central carbon. Such conformational relaxation is active at human body temperature, and may thus be potentially relevant for the mechanism of action of the drug. Our study shows that the comparative study of the relaxation map of related molecular species is a powerful tool to identify and classify secondary relaxation processes. The amorphous drug is found to be unstable against recrystallization at as well as slightly below room temperature, and to display-two-dimensional growth with only sporadic nucleation, characterized by an Avrami kinetic exponent of 2.05 ± 0.05. The kinetic stability of the amorphous form of mitotane, observed at room temperature in micellar formulations, is therefore limited to the nanoconfined sample and is not observed in the bulk compound.

1. Introduction

The poor aqueous solubility of active pharmaceutical ingredients (APIs) is one of the major challenges facing the pharmaceutical industry. It is well known that molecular glasses in general, and amorphous small-molecule APIs in particular, display higher solubility and faster dissolution rates in solvents compared with crystalline phases, due to the fact that disorder entails a higher free energy density and thus a lower barrier for dissolution. At the same time, however, the glass phase is prone to recrystallization, a process which must be avoided to maintain the solubility and thus bioavailability advantage of the amorphous phase (Craig et al., 1999; Gupta et al., 2004; Bhardwaj et al., 2013; Ruiz et al., 2017).

Glasses are normally formed from the liquid phase, either by fast evaporation of a solvent in a solution or by fast-cooling the molecular melt below the melting point (supercooled liquid). Understanding the formation of the glass state requires knowledge of the so-called cooperative structural relaxation, whose kinetic arrest marks the glass transition temperature T_g, and whose sensitivity to temperature variations determines how easily the glass state can be obtained (Tanaka, 2005) as well as the so-called dynamic fragility index (Angell, 1985) of the glass former (see Section 3.2), which is potentially related to the crystallization tendency in the supercooled liquid state.

On the other hand, understanding the kinetic stability of the glass, which is a non-equilibrium phase of matter continuously evolving toward higher-density and lower-free-energy states, implies a knowledge of the local (secondary) relaxation processes occurring in the glass (Zhou et al., 2002; Gupta et al, 2004; Bhardwaj et al., 2013). It has been shown, for example, that the kinetic stability of glassy APIs can only be achieved below the activation temperature of whole-molecule secondary

* Corresponding author.
E-mail address: michela.romanini@upc.edu (M. Romanini).

https://doi.org/10.1016/j.ijpharm.2022.122390
Received 29 July 2022; Received in revised form 7 November 2022; Accepted 8 November 2022
Available online 13 November 2022

relaxations (Kissi et al., 2018). Similarly, glassy polymers show poorer mechanical properties when antiplasticizing fillers are added, which are molecular additives that inhibit secondary relaxations and reduce the kinetic fragility of the polymeric glass former (Riggleman et al., 2007; Mascia et al., 2020).

Here we analyze the molecular relaxations and crystallization kinetics of the amorphous state of mitotane (*o,p'*-DDD or *o,p'*-dichlorodiphenyldichloroethane, commercialized in tablets under the trade name of Lysodren®), a drug used for the treatment of Cushing's syndrome, and the only chemotherapeutic agent approved for the non-surgical treatment of adrenocortical carcinoma (Hutter and Kayhoe, 1966; Temple et al., 1969), a rare but aggressive malign tumor representing 0.2 % of deaths due to cancer in the world. Mitotane is one of the isomers present in DDD, a halogenated organic insecticide practically insoluble in water which is derived from the well-known DDT pesticide and consists of a mixture of different structural isomers, of which one of the most abundant ones is mitotane (Cueto and Brown, 1958).

The efficacy of mitotane is limited due to unfavorable biopharmaceutical properties and dose-limiting toxicity. Crystalline mitotane is a white powder soluble in ethanol, ether and CCl_4 and almost insoluble in water (solubility: $1.29 \cdot 10^{-7}$ mol/l at 25 °C) (Biggar and Riggs, 1974; Attivi, 2010). Oral absorption is poor and variable between patients (Takano et al., 2008), and bioavailability is estimated to be less than 40 %, likely due to poor solubility and poor absorption in the intestine (Moy, 1961; Moolenaar et al., 1981). It has also been reported that therapeutic serum levels of mitotane may take several months to be achieved (Terzolo et al., 2013).

It is therefore crucial to devise strategies to improve the solubility and bioavailability of mitotane (Haider et al., 2021). An early study showed that the absorption of mitotane can be improved through control of its galenic formulation (Watson et al., 1987), and more recent studies have focused on the development and characterization of self-microemulsifying drug delivery systems, nanosuspensions, and polymer-based micellar formulations (Musial et al., 1985; Trotta et al., 2001; Attivi et al., 2010; Battung et al., 2013; Hassan, 2015; Haider et al., 2020). The most recent study (Haider et al., 2020) has shown that mitotane encapsulated inside polymer-based micelles of 40 nm in diameter remains in the supercooled liquid phase at least during 15 days at room temperature, that is, more than 40 K above the glass transition temperature of the compound (see Section 2). According to these Authors, this route is a promising tool to solve the poor bioavailability of mitotane (Hassan, 2015; Haider et al., 2020).

Here, we carry out a scanning calorimetry and dielectric spectroscopy characterization of mitotane as well as of a closely related compound, *o,p'*-dichlorobenzophenone (see the inset to Fig. 1 for the molecular structures). The scope of the present work is to study the molecular relaxation dynamics, glass transition, kinetic fragility, and the crystallization tendency and kinetics, of bulk liquid mitotane, to determine whether the reported metastability of micellar formulations of this compound (Haider et al., 2020) is common also to the bulk material, or whether it is an effect of geometrical confinement or of hetero-interactions, and to investigate a possible correlation between crystallization time and structural relaxation dynamics. A second goal is the identification of local relaxation processes in mitotane. For this purpose, the intramolecular relaxation process of mitotane is compared with that of *o,p'*-dichlorobenzophenone and that of the recently characterized *o*-bromobenzophenone glass former (Romanini et al., 2021). We show that such comparison allows identifying secondary relaxations in mitotane and related halogenated diphenyl moieties, and provides useful information on molecular processes that are active also when mitotane is dissolved in a biological solution and that may thus play a role for the mechanism of action of this drug.

2. Material and methods

Mitotane (racemic mixture of two chiral enantiomers) and *o,p'*-dichlorobenzophenone, both with purity better than 98 %, were purchased from Sigma-Aldrich and used as received. Differential scanning calorimetry (DSC) experiments were carried inside aluminum pans, by means of a Q100 from TA Instruments working in controlled nitrogen atmosphere with a flow rate of 25 ml/min. Heat-cool cycles were performed with a heating/cooling rate of 10 K/min and sample masses of about 10 mg (a microbalance sensitive to 0.01 mg was employed for mass determinations). Details of the temperature and enthalpy calibration of the device have been given elsewhere (Barrio et al., 2009).

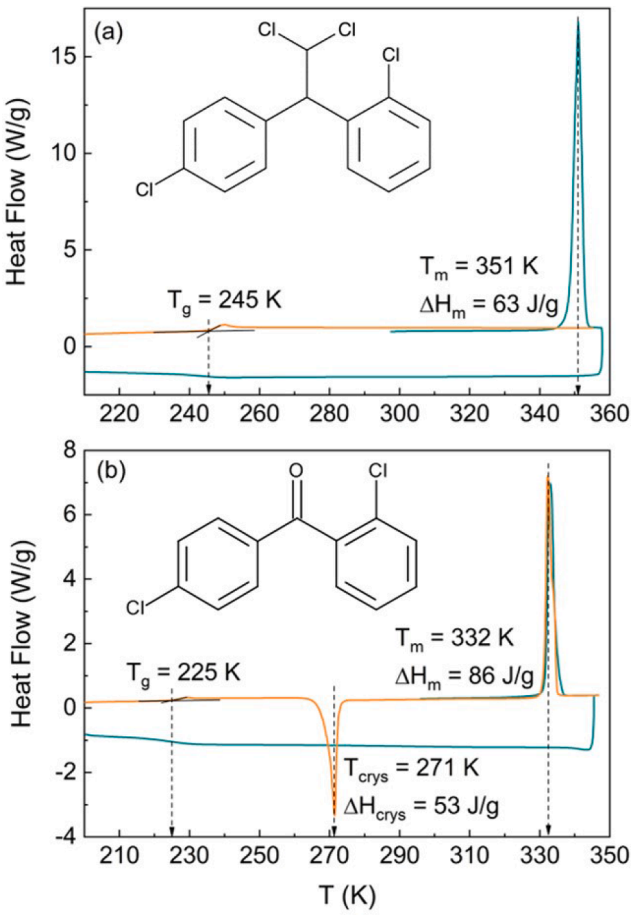

Fig. 1. DSC traces of mitotane (a) and *o,p'*-dichlorobenzophenone (b), measured upon heating the polycrystalline powder, then cooling from the liquid state into the glass state (blue curves), and subsequently heating up the sample from the glass state (orange curves). Glass transition temperatures, as well as melting and recrystallization temperatures and enthalpies are indicated (in the case of *o,p'*-dichlorobenzophenone, the second-heat melting is virtually identical to the first). Insets: molecular structures of the two glass formers studied. (For interpretation of the references to colour in this figure legend, the reader is referred to the web version of this article.)

For dielectric spectroscopy measurements, the samples were placed in a stainless steel parallel-plate capacitor specially designed for the characterization of liquid samples. Temperature control of the capacitor was achieved with a nitrogen-gas flow cryostat (Novocontrol Quatro cryosystem) with an accuracy of 0.1 K. The as-received powders were melted directly inside the capacitor, and silica spacers of 50 μm diameter were employed to keep the two electrodes at fixed distance.

Isothermal complex relative permittivity spectra were acquired with a Novocontrol Alpha analyzer by increasing the temperature in a stepwise fashion. Spectra were recorded in the frequency range between 10^{-2} and 10^{6} Hz. To obtain relaxation times and quantify the changes in relaxation dynamics, we fitted the dielectric loss spectra (imaginary part of the complex permittivity spectra) as the sum of a frequency power law, corresponding to the dc conductivity contribution of the sample,

and a model function for each relaxation component. For data acquisition and fitting, we used the WinData and WinFit programs provided for this purpose by the manufacturer (Novocontrol). The model function was the imaginary part a Havriliak-Negami function, whose analytical expression is (Havriliak and Negami, 1967):

$$\varepsilon^*(\omega) = \varepsilon_\infty + \frac{\Delta\varepsilon}{(1+(i\omega\tau_0)^a)^b} \quad (1)$$

Here $\omega = 2\pi\nu$ is the angular frequency, ε_∞ is the permittivity in the high frequency limit, $\Delta\varepsilon$ is the dielectric intensity or strength, the exponents a and b are shape parameters that can vary between 0 and 1, and τ_0 is a time parameter connected to the characteristic relaxation time τ, corresponding to the maximum of the relaxation time distribution. In terms of the fit parameters, τ is given by:

$$\tau = \tau_0 \left[\sin\left(\frac{a\pi}{2b+2}\right)\right]^{-1/a} \left[\sin\left(\frac{ab\pi}{2b+2}\right)\right]^{1/a} \quad (2)$$

The exponents a and b were initially let free to vary to adjust to the shape of the loss curves. This procedure showed that primary relaxations had an asymmetric line shape that could be well described by a Havriliak-Negami function with both a and b different from unity in the case of mitotane, while for the case of dichlorobenzophenone a Cole-Davidson function was sufficient, which is a special case of Eq. (1) with $a = 1$ and b less than 1. Instead, all secondary relaxations had a broad symmetric profile, best described by a Cole-Cole function (Cole and Cole, 1942), which corresponds to a special case of Eq. (1) with $b = 1$, in which case the relaxation time is simply equal to τ_0.

Optical microscope images were obtained by means of an Olympus BX51 fluorescence microscope equipped with a video camera, using a 10-fold magnification and white back-illumination.

3. Results and discussion

3.1. Differential scanning calorimetry (DSC) characterization

Fig. 1 shows the calorimetric heat-cool-heat traces of mitotane (a) and *o,p'*-dichlorobenzophenone (b). The (very similar) molecular structures of both compounds are shown as insets. The melting points (T_m) of both substances (332 K for *o,p'*-dichlorobenzophenone and 351 K for mitotane) are in agreement with known values (Bradley et al. 2014). Upon cooling from the liquid phase, both compounds could be supercooled to the glass state, as visible in the cool-down part of the DSC curves as well as in the second heat-up scans, where the typical specific-heat discontinuity associated with the glass transition is detected. The glass transition temperatures (T_g) were determined from the onset of the glass transition feature in the second heat-up scan, as indicated in Fig. 1, and turned out to be 225.0 ± 1.0 K for *o,p'*-dichlorobenzophenone and 245.5 ± 1.0 K for mitotane, respectively. It may be observed that supercooled liquid *o,p'*-dichlorobenzophenone crystallizes upon heating from the glass state, with a recrystallization onset about 40 K above T_g, while mitotane does not recrystallize during our DSC experiments.

The higher values of T_g and T_m of mitotane ($M_w = 320$ g mol^{-1}) are in agreement with its larger molecular mass compared to *o,p'*-dichlorobenzophenone ($M_w = 251$ g mol^{-1}). At the same time, however, it is interesting to remark that the melting point of *o,p'*-dichlorobenzophenone is more than 40 K higher than that of the almost isobaric (actually heavier) compound *o*-bromobenzophenone ($T_m = 299$ K and $M_w = 261$ g mol^{-1}; the mass of a bromine atom is slightly more than twice that of the chlorine atom), and it is less than 10 K smaller than that of the significantly heavier mitotane compound. Similarly, the glass transition temperature of *o*-bromobenzophenone is 211 K (Romanini et al., 2021), which is lower than that of *o,p'*-dichlorobenzophenone. This suggests that intermolecular interactions are significantly stronger in the case of *o,p'*-dichlorobenzophenone compared with the other two compounds, which may be expected as the latter is the only molecule of the three capable of forming hydrogen bonds, namely between the ketone oxygen and the chlorine atoms (the ketone group is absent in mitotane, and bromine is not capable of forming H-bonds in the liquid state). The importance of such interactions in *o,p'*-dichlorobenzophenone is corroborated also by the fact that the T_g of the three compounds follows the same order as their respective melting points, that is, it does not scale with the (square root of) the molecular mass as experimentally observed for van-der-Waals liquids (Novikov, and Rössler, 2013). Interestingly, many benzophenone derivatives, including *o*-bromobenzophenone, *o,p'*-dichlorobenzophenone, and benzophenone itself, have a very strong tendency to crystallize in the supercooled liquid state, leading to fast recrystallization also very close to T_g (Romanini et al., 2021).

3.2. Molecular relaxation processes

Fig. 2 shows selected isothermal loss spectra of both mitotane (a) and *o,p'*- dichlorobenzophenone (b) in the amorphous state, namely both in the glass state below T_g and in the supercooled liquid state above T_g. Several loss components can be detected in these series of spectra, visible either as local maxima (structural relaxation) or as shoulders to the high-frequency side of the maximum (secondary relaxations).

In order to extract characteristic relaxation times and shape parameters of the loss processes, we fitted all spectra as the sum of several components (see Section 2). Representative fits of the loss spectra of both studied compounds are shown in Fig. 3.

The Arrhenius relaxation maps of both compounds, resulting from

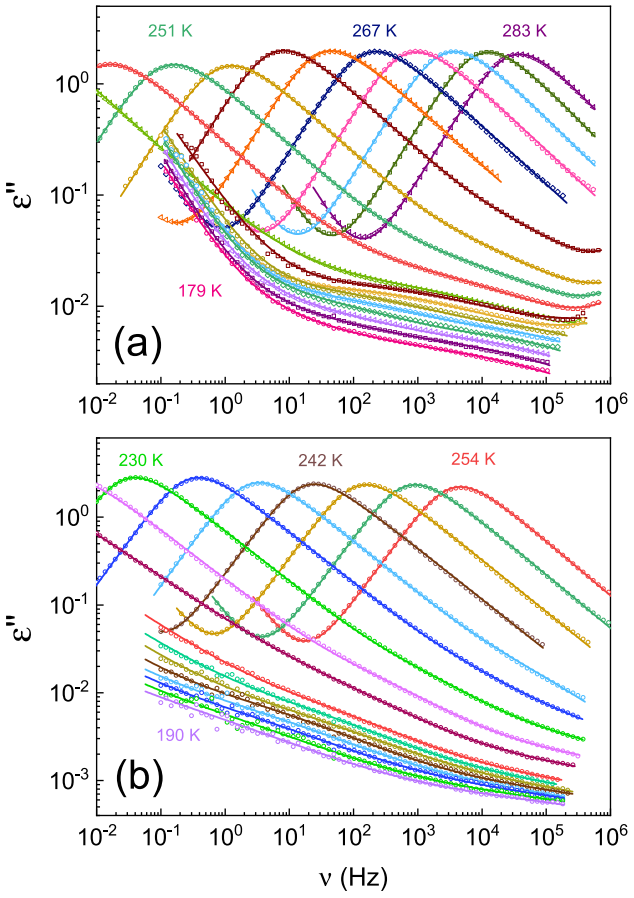

Fig. 2. Selected isothermal loss spectra of amorphous mitotane (a) and *o,p'*-dichlorobenzophenone (b), acquired with an increasing temperature ladder. Spectra in (a) are shown every 8 K between 179 and 235 K, and every 4 K between 243 and 283 K. Spectra in (b) are shown every 4 K between 190 and 254 K.

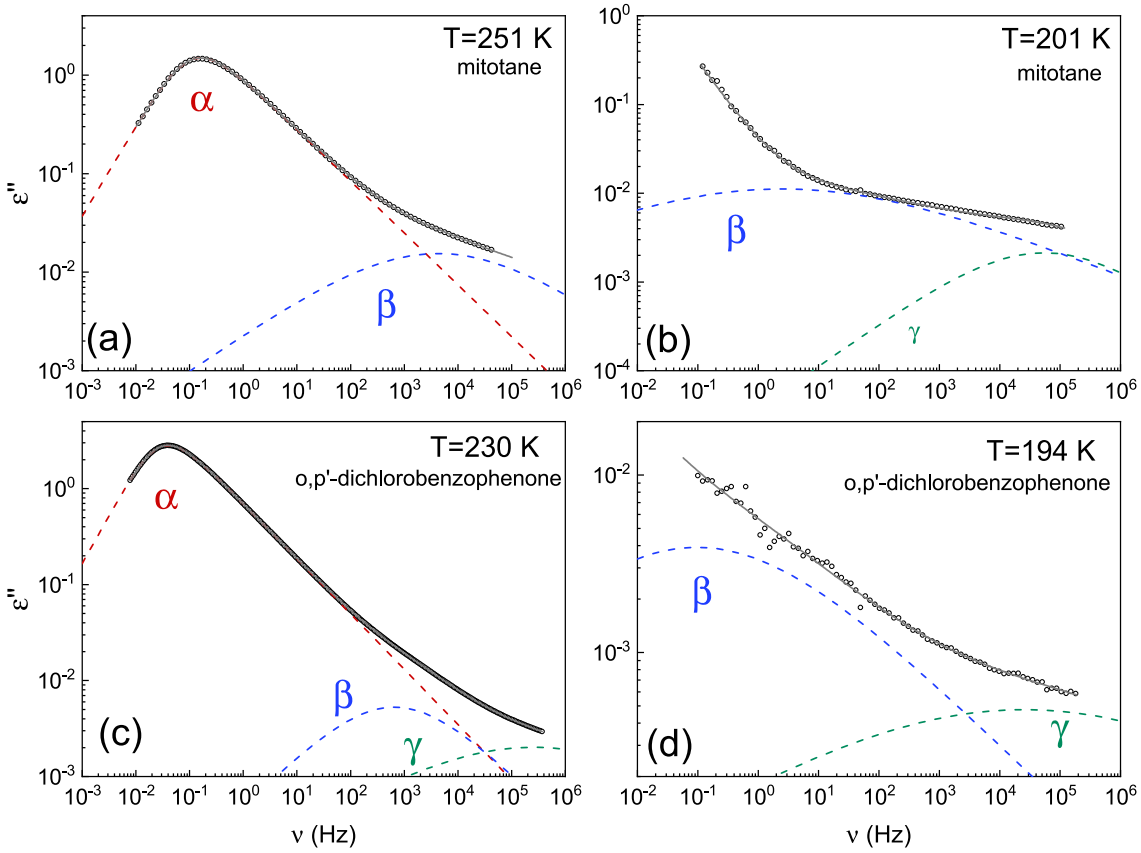

Fig. 3. Fit of the loss spectra of mitotane at 251 (a) and 201 K (b), and of those of *o,p'*-dichlorobenzophenone at 230 (a) and 194 (b) K. Greek letters indicate the relaxation process corresponding to each fit component.

the fit procedure applied to all measured spectra, are shown in Fig. 4. The structural relaxation time of both compounds displays a positive curvature as a function of the inverse temperature, which could be modeled by means of the modified Vogel–Fulcher–Tammann (VFT) equation (Angell, 1988):

$$\tau_\alpha(T) = \tau_\infty exp\left(D\frac{T_{VF}}{T - T_{VF}}\right) \tag{3}$$

Such fit yielded, for supercooled liquid mitotane, a dynamic glass transition temperature (defined as the temperature at which the structural relaxation time reaches 100 s) of 243 ± 1 K, and an activation energy at T_g of 316 kJ mol^{-1}. The corresponding values for *o,p'*-dichlorobenzophenone were T_g = 224 ± 1 K and $E_a(T = T_g)$ = 248 kJ mol^{-1}. The dynamic glass transition temperatures obtained by dielectric spectroscopy were thus only slightly lower than the calorimetric ones, as it is often found experimentally.

The kinetic fragility index of the structural relaxation, a dimensionless parameter which describes the deviation of the structural relaxation from a simple Arrhenius law, is defined as (Angell, 1985; Böhmer et al., 1993):

$$m = \left.\frac{d(\mathrm{Log}\tau_\alpha)}{d(T_g/T)}\right|_{T=T_g} = \frac{DT_{VF}T_g}{(T_g - T_{VF})^2\, ln10} \tag{4}$$

The second equality in Eq. (4) holds if the structural relaxation time follows the VFT Eq. (3). The fragility indices were 68 ± 2 for mitotane and 58 ± 2 for *o,p'*-dichlorobenzophenone, respectively, indicating that both compounds are relatively strong glass formers.

In contrast to the structural relaxation, the secondary relaxations of both compounds were characterized by a simply-activated (Arrhenius) temperature dependence, as evidenced by the quality of the straight-line fits in both panels of Fig. 4. Secondary relaxations are of two types: they may correspond either to intramolecular relaxation processes (*e.g.*, interconversions between different molecular conformers, inversion dynamics of flexible rings, or reorientation of side groups) (Hellwig et al., 2020; Valenti et al., 2021), or else, they can stem from the local (subdiffusive), whole-molecule rototranslational relaxation dynamics known as Johari-Goldstein relaxation and which corresponds to the non-cooperative version of the molecular motion responsible for the structural relaxation (Romanini et al., 2017; Caporaletti et al., 2019).

The β relaxation time displayed a dynamic cross-over with a clear-cut change of slope at T_g. Such feature is a common one of Johari-Goldstein processes (Ngai and Paluch, 2004). The activation energy of the β process below T_g was found to be 45 ± 1 kJ mol^{-1} for mitotane and 68 ± 1 kJ mol^{-1} for *o,p'*-dichlorobenzophenone, respectively. The comparative Arrhenius plot of mitotane and *o,p'*-dichlorobenzophenone is shown in Fig. 5(a) to allow visual comparison of the curvature of the structural relaxations and slopes of the secondary relaxations.

To confirm the Johari-Goldstein origin of the secondary β process of both glass formers, we have compared the experimental relaxation times with the predictions of the Coupling Model (Ngai, 1998; 2007). According to such model, the relaxation time of a Johari-Goldstein at a given temperature T should be a function only of the parameters of the structural (α) relaxation of the same compound at the same temperature, and should match approximately the so-called precursor time, given by:

$$\tau_{CM}(T) = t_c^{\,1-w}\tau_\alpha(T)^w \tag{5}$$

Here, t_c is a universal characteristic time equal to $2 \cdot 10^{-12}$ s for both molecular and macromolecular glass formers (Ngai and Paluch, 2004), τ_α is the structural relaxation time, and w is the exponent of the Kohlrausch–Williams–Watts function that describes the structural loss feature in the time domain, and which is well approximated (Alvarez et al., 1991; 1993) by $w = (ab)^{1/1.23}$, where a and b are the Havriliak-

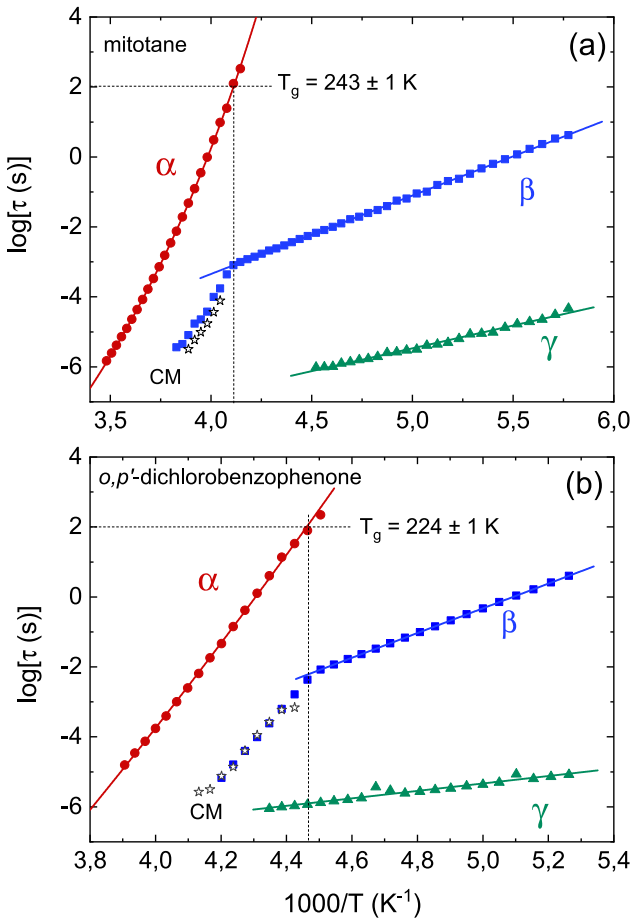

Fig. 4. Arrhenius relaxation map for mitotane (a) and *o,p'*-dichlorobenzophenone (b). In each panel, circles represent the structural α relaxation, squares the Johari-Goldstein β relaxation, and triangles the conformational γ relaxation. Continuous lines are fits. Stars correspond to the precursor relaxation time calculated from the Coupling Model (see the text for details).

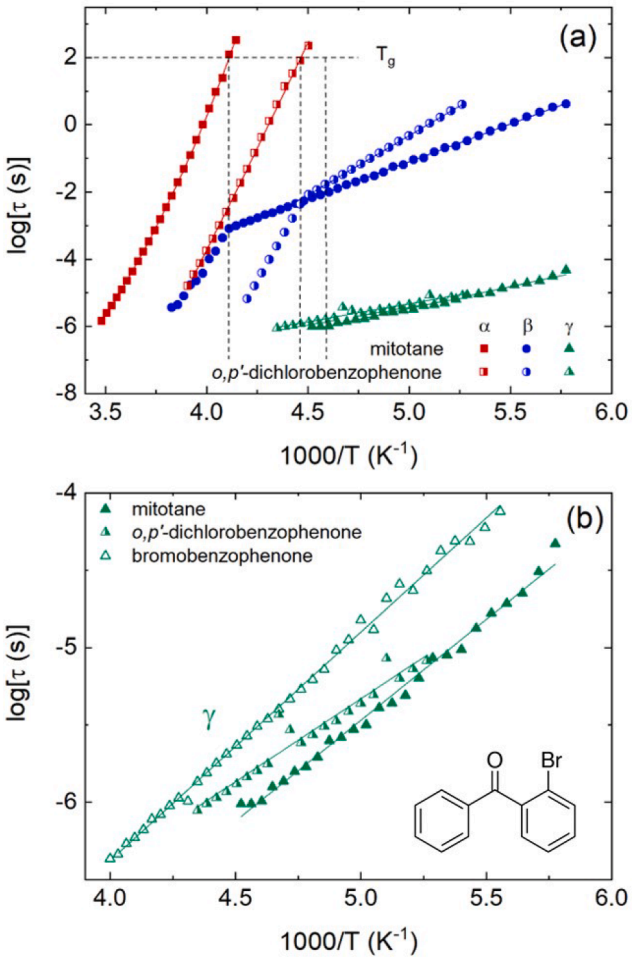

Fig. 5. (a) Comparative Arrhenius plots of mitotane and *o,p'*-dichlorobenzophenone. (b) Arrhenius plot of the intramolecular relaxation of both compounds, compared also with published data on *o*-bromobenzophenone (after Romanini et al., 2021). The inset to (b) shows the molecular structure of the latter compound.

Negami exponents describing the structural loss feature in the frequency domain (see Section 2).

As it can be observed in the relaxation map of Fig. 4, the precursor time τ_{CM} matches rather well the experimental relaxation times of the β process at and slightly above T_g, which corresponds to the expected range of validity of the Coupling Model. This shows that the β relaxation is a whole-molecule Johari-Goldstein process. Correspondingly, the γ relaxation arises from an *intramolecular* process.

Given the relative rigidity of the conjugated aryl rings of the mitotane molecule, such intramolecular process must correspond to the rigid rotation of a side group with respect to the covalent bond linking it to the central carbon atom. In order to be visible in dielectric spectroscopy, such rotation has to involve the variation in the magnitude or orientation of the molecular dipole moment. This excludes the possibility that the γ relaxation stems from the rotation of the chlorophenyl ring with the halogen substituent in the 4-position, around its peripheral bond to the rest of the molecule, because such a rotation leaves invariant the position of the chlorine atom and therefore does not entail any change in molecular dipole moment. On the other hand, the internal rotation of the dichloromethane group is too fast to be detected in our experimental frequency range, as such motion is usually observed only in the ps time range (that is, at frequencies of hundreds of GHz or even in the THz range) (Crossley and Smyth, 1969) and its characteristic frequency varies only slowly with temperature, as in the case of halogenated ethane derivatives (Madan, 1975).

This leaves as the only possible origin for the γ relaxation the reorientation of the aryl ring with the chlorine substituent in the 2-position. This assignment of the γ process is further corroborated by comparison between the two glass formers studied, and the related *o*-bromobenzophenone compound which was the topic of a previous publication by some of us (Romanini et al., 2021). The comparative Arrhenius plot of the γ relaxations in mitotane, *o,p'*-dichlorobenzophenone, and *o*-bromobenzophenone is shown in Fig. 5(b). The activation energies of the γ process are 25 ± 1 kJ mol^{-1} for mitotane, 21 ± 2 kJ mol^{-1} for *o,p'*-dichlorobenzophenone, and 28 ± 1 kJ mol^{-1} for *o*-bromobenzophenone, respectively. The γ relaxation times are almost identical in mitotane and *o,p'*-dichlorobenzophenone, despite the very large difference in the structural (α) relaxation times of the two compounds (see Fig. 5(a)). This lack of correlation between γ and α relaxation times is expected for an intramolecular secondary process, as the intramolecular interconversion dynamics is independent of the viscosity and thus of the structural mobility (Romanini et al., 2018).

The coincidence of relaxation times confirms that the γ relaxation arises from the same microscopic dynamic process in both compounds, namely, the rigid rotation of the aryl ring with the chlorine atom in the 2-position. The data for *o*-bromobenzophenone reveal instead a slightly slower γ relaxation (Fig. 5(b)). This is actually to be expected, both because of the larger mass of the bromophenyl ring compared to the chlorophenyl one, and because in the case of *o*-bromobenzophenone a more pronounced electronic resonance stabilizes the coplanar conformation of the ketone-phenyl moiety (Romanini et al., 2021). (Contrary

to mitotane and *o,p'*-dichlorobenzophenone, the *o*-bromobenzophenone molecule possesses an unsubstituted phenyl group, which favors a ground-state conformation with extended conjugation between the ketone and phenyl moieties).

It is worth stressing that the γ relaxation is active also at and above room temperature. Since previous studies have shown that intramolecular relaxations are not influenced by the local environment in the liquid or amorphous phase (Romanini et al., 2018, 2021; Valenti et al., 2019, 2021), this implies that mitotane exists, in the human body, in different conformational states that are rapidly interconverted into one another. Moreover, the fact that also closely related chemical compounds such as *o,p'*-dichlorobenzophenone display exactly the same process with the same characteristic time, indicates that also mitotane derivatives such as the pharmacologically active acyl chloride metabolite of mitotane, which preserves the di-chlorophenyl moiety of the parent compound (Nelson and Woodard, 1949; Fang, 1979), should display the same intramolecular relaxation. This fact has important consequences for the effective molecular shape and steric interactions of active mitotane metabolites, and thus potentially also for the mechanism of action of the drug, which is still debated (Waszut et al., 2017). Indeed, the conformational disorder entails that the hydration shell surrounding mitotane has a more dynamic character than the hydration shell surrounding a rigid hydrophobic solute, which leads to a reduction of orientational entropy of hydration water molecules. It moreover entails that, in particular in the proximity of other biomolecules where the drug loses partially its hydration shell, it effectively occupies a larger volume and displays larger steric hindrance than a similar drug without conformational dynamics. Lastly, the conformational dynamics may be important as it bestows the drug a flexibility that may facilitate the induced-fit interaction at the active site of the target.

3.3. Isothermal crystallization of supercooled liquid mitotane

Fig. 6 shows three series of isothermal spectra acquired at fixed temperature on supercooled liquid mitotane, during the isothermal transformation to the thermodynamically stable crystalline phase. Of the three temperatures studied, one corresponds approximately to room temperature (289 K), while the other were chosen to explore the kinetic stability of the supercooled liquid in typical refrigerated storage conditions in a fridge (279 and 284 K).

The real and imaginary permittivity spectra acquired at different times at these temperatures are shown in the upper and lower panels of Fig. 6, respectively. As time progresses, the loss feature of the structural relaxation (lower panels) decreases in intensity due to the removal of molecular species in the liquid phase in favor of the crystalline phase, which obviously does not display any molecular relaxation in the studied frequency range, and correspondingly, the static permittivity (low-frequency plateau value of the real permittivity spectra, upper panels) decreases. DSC characterization on the fully recrystallized supercooled liquid mitotane (not shown) shows a melting point identical to that of the as-received powder, which indicates that mitotane recrystallized in its known crystalline structure (no polymorphism is known for the mitotane racemate) (Arora and Bates, 1976).

Fig. 7(a) shows the static relative permittivity as a function of time during the isothermal cold crystallization measurements. The static permittivity is defined for this purpose as the real part of the complex permittivity spectrum at the fixed frequency of 1.5 kHz for the isothermal series of spectra at 289 K, and at the frequency of 0.2 kHz for the isothermal series at 279 and 284 K. These frequencies are defined in order that the static permittivity corresponds to the plateau value characterizing the real-permittivity spectra at low frequencies. It can be observed in Fig. 7(a) that the static permittivity has initially a constant value corresponding to the dielectric constant of liquid mitotane at each temperature. After an onset time, the static permittivity decreases as the crystallization progresses. As shown in Fig. 7(a), we define the onset time t_o as the intersection between the horizontal line marking the static permittivity value of the supercooled liquid, and the tangent to the decreasing portion of the graph in the initial moments of crystallization.

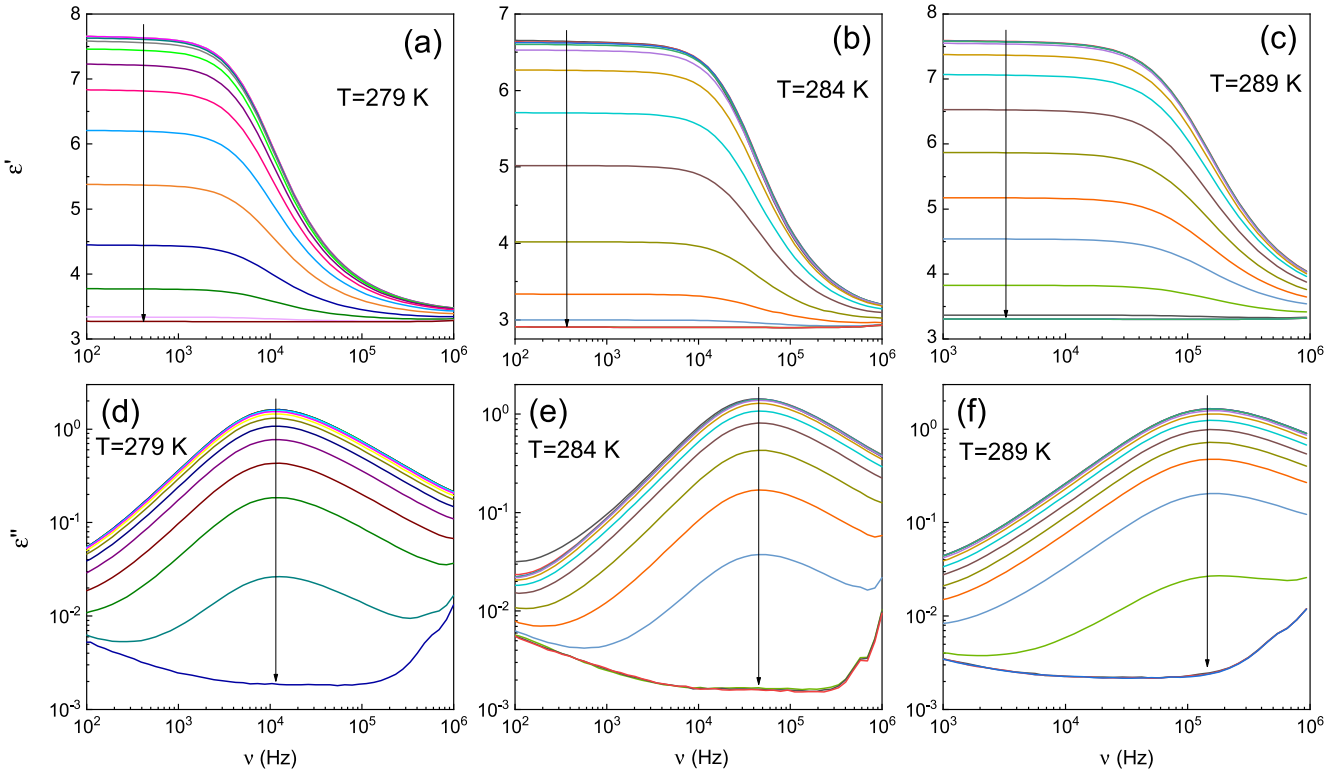

Fig. 6. Real (upper panels) and imaginary (lower panels) permittivity spectra of mitotane during isothermal crystallization of the supercooled liquid at three different temperatures, namely 279 (panels (a) and (d)), 284 (panels (b) and (e)), and 289 K (panels (c) and (f)).

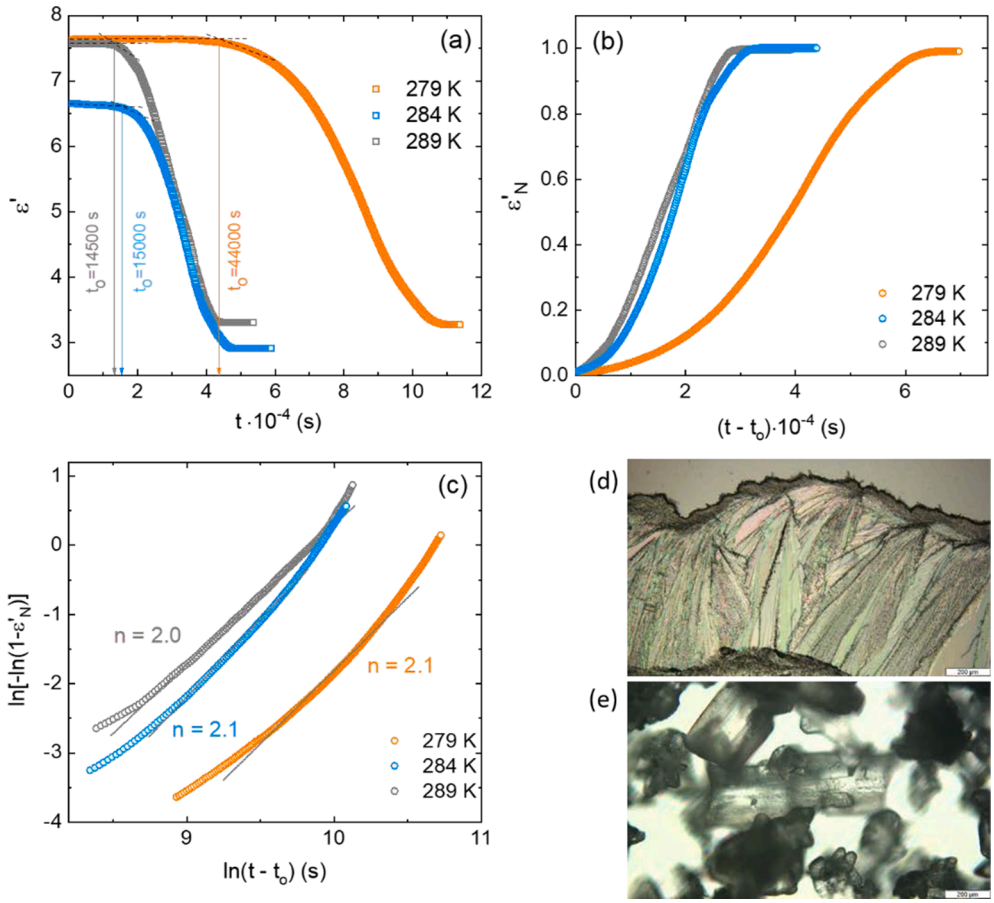

Fig. 7. Static permittivity (a), normalized permittivity difference (b), and Avrami plots (c) for the crystallization process of mitotane at the temperatures of 279 (orange), 284 (blue), and 289 (grey) K. (d,e) Optical microscope images of a mitotane sample crystallized from the melt (d) and of the as-received mitotane polycrystalline powder (e). (For interpretation of the references to colour in this figure legend, the reader is referred to the web version of this article.)

In order to study the kinetics of crystallization, we define as customary (D'Amore et al., 1990) a time-dependent, normalized static permittivity difference as:

$$\varepsilon'_N(t) = \frac{\varepsilon'(t_o) - \varepsilon'(t)}{\varepsilon'(t_o) - \varepsilon'(t_\infty)} \tag{6}$$

Here, $\varepsilon'(t_o)$ is the value of the static permittivity at the onset time of crystallization, that is, the dielectric constant of supercooled liquid mitotane, $\varepsilon'(t_\infty)$ is the corresponding value at very large times (after the end of the crystallization process), which represents the dielectric constant of crystalline mitotane, and $\varepsilon'(t)$ is the static permittivity as a function of time. The quantity ε'_N is plotted as a function of time in Fig. 7 (b).

According to the Avrami model (Avrami 1939; 1940), after the onset time the normalized static permittivity difference should decrease over time as:

$$\varepsilon'_N(t) = 1 - \exp\{-k(t-t_o)^n\} = 1 - \exp\{-[K(t-t_o)]^n\} \tag{7}$$

Here, n is the Avrami exponent (also known as Avrami constant), which depends on the morphology of the growing crystallites and the on their exact growth mechanism, k is a rate constant, and K is the crystallization rate in inverse seconds, related to the previous quantities as $K = k^{1/n}$ (Yousefzade et al., 2019).

If the Avrami equation is obeyed, the plot of the quantity $\ln[-\ln(1-\varepsilon'_N(t))]$ should have a linear dependence on the variable $\ln(t-t_o)$, with slope equal to the Avrami exponent. Fig. 7(c) shows that such Avrami plot indeed yields a straight-line dependence, with virtually equal slope of 2 for all three crystallization temperatures studied. Table 1 summarizes the Avrami parameters obtained in each case.

Table 1
Static permittivity difference (ε_{liquid}-$\varepsilon_{crystal}$) and Avrami parameters for the isothermal crystallization of supercooled liquid mitotane.

Temperature [K]	ε_{liquid}– $\varepsilon_{crystal}$	n	K [s^{-1}]
279	4.4	2.1	5.0·10^{-5}
284	3.8	2.1	2.3·10^{-5}
289	4.3	2.0	1.9·10^{-5}

The optical microscope image of a mitotane sample crystallized from the supercooled liquid is displayed in Fig. 7(d). The observed crystallites display a lamellar structure, corresponding to a two-dimensional growth. The experimental value of 2 of the Avrami exponent can then be rationalized, for two-dimensional growth, assuming that nucleation of the crystalline phase is sporadic and takes place fundamentally only prior to the growth of crystallites that have nucleated simultaneously, without further nucleation processes during the growth of the existing crystallites (Wunderlich 1976; Tripathi et al., 2015). The micrograph of Fig. 7(e) shows the typical shape of thin crystallites present in the (as-received) mitotane powder sample. It may be observed that such crystallites have a comparable size in two spatial dimensions, while their size is smaller in the third direction (orthogonal to the plane of sight). This macroscopic shape is consistent with a mainly bidimensional growth of crystalline nuclei.

Interestingly, the recrystallization of mitotane from the supercooled liquid state is significantly slower than the overall crystallization rate of the related benzophenone derivatives. In fact, recrystallization of benzophenone is so fast that the glass transition has to be obtained by fast quenching from above the melting point (Romanini et al., 2021). It

would therefore seem that replacement of the ketone group of the central carbon atom of benzophenone and its derivatives, with the chloromethyl group present in mitotane, results in a significantly lower crystallization tendency.

Our isothermal crystallization results indicate that bulk supercooled liquid mitotane is unstable against recrystallization at room temperature. Therefore, it is the nanoconfinement in micellar dispersions that is responsible for the kinetic metastability of the supercooled liquid phase of recently reported mitotane formulations (Haider et al., 2020). Recent studies of organic glass formers under geometrical confinement indicate that the structural relaxation is suppressed in nanoconfined liquids where molecules form only small clusters and only the Johari-Goldstein relaxation is present (Ngai et al., 2019, 2020; Ruiz et al., 2019). The metastabilization of micellar mitotane at room temperature may therefore be favored by the suppression of the structural relaxation of mitotane in nanoscopic domains, where only the faster and less cooperative Johari-Goldstein and intramolecular relaxation processes may be active.

Fig. 8 displays the logarithmic correlation between the partial crystallization time of mitotane, defined as the time required for isothermal crystallization of 25 % of the sample, measured from the crystallization onset, and the structural (α) relaxation time at the same temperature. In the same log–log plot we show for comparison the corresponding data of three other active pharmaceutical ingredients (stiripentol, indomethacin and celecoxib) (Mehta et al., 2016; Ruiz et al., 2017) as well as own data on the 2-benzylphenol glass former, slightly above their respective glass transition temperatures.

The two characteristic times are correlated, in the sense that the longer the structural relaxation time, the longer also the crystallization time. This behavior is expected to be valid only near (more precisely, slightly above) the glass transition temperature T_g, while at higher temperature molecular mobility is not the limiting kinetic factor for the crystallization process (Romanini et al., 2019). Even restricting the temperature range to a narrow range above T_g, however, it is apparent from the comparison with other glass formers that this correlation does not have a universal character, since the slope of the log–log plot for mitotane (0.4) is significantly smaller than (virtually, half the value of) that of other studied drugs (0.8). It is worth noting that also in the case of 2-benzylphenol (own data), the slope of the plot of Fig. 8 is considerably

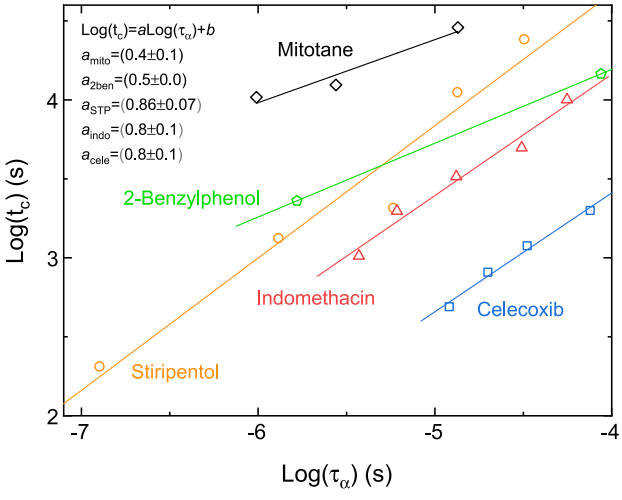

Fig. 8. Isothermal crystallization time to reach 25 % of crystallized sample (t_c), plotted as a function of the structural relaxation time at the same temperature for mitotane (rhombs, T_g = 245 K), as well as for several molecular glass formers: 2-benzylphenol (pentagons, T_g = 220 K), stiripentol (circles, T_g = 246 K), indomethacin (triangles, T_g = 318 K), and celecoxib (squares, T_g = 328 K). Values for stiripentol were obtained from Ruiz et al. (2017), those for indomethacin and celecoxib from Mehta et al. (2016), and those for 2-benzylphenol are our own data. Continuous lines are linear fits.

smaller (0.5) than for previously studied compounds. This confirms that the above-mentioned correlation is compound-specific rather than quantitatively universal to all molecular glass formers.

4. Conclusions

We employed broadband dielectric spectroscopy to investigate the glass transition, molecular relaxation dynamics, and recrystallization kinetics of amorphous mitotane, and complemented our dielectric characterization with the help of differential scanning calorimetry and optical microscopy investigations. To identify and analyze the molecular dynamic processes, we compare the relaxation dynamics of mitotane with that of a closely-related molecule, *o,p'*-dichlorobenzophenone.

Supercooled liquid mitotane displays a structural relaxation characterized by relatively low fragility index, as well as a Johari-Goldstein relaxation with characteristic time in agreement with the predictions of the Coupling Model. In addition, mitotane displays an intramolecular relaxation in the glass phase. By comparison with the relaxation dynamics of the *o,p'*-dichlorobenzophenone derivative, we identify such intramolecular relaxation as the internal rotation of one of the chlorobenzene rings of the mitotane molecule, the one with the chlorine in position 2. The intramolecular relaxations of both mitotane and *o,p'*-dichlorobenzophenone have the same activation energy, and at a given fixed temperature their intramolecular relaxation times coincide almost perfectly and are only slightly shorter than those of the *o*-bromobenzophenone molecule, resulting in a perfect overlap of intramolecular relaxation times in the Arrhenius plot. This shows that the comparative study of the relaxation map of related molecular species is a powerful tool to identify secondary relaxation processes. Furthermore, the fact that the same intramolecular relaxation is observed in similar molecules containing the same chlorophenyl ring strongly suggests that the same process is active also in the pharmacologically active acyl chloride metabolite of mitotane, which preserve the two-ring moiety of the parent compound. Such inter-conformer relaxation dynamics is active below and above T_g, and, due to the insensitivity of intramolecular relaxations to the local environment, it is expected to display the same relaxation rate also in solutions of mitotane or mitotane acyl chloride. This entails that these active pharmaceutical ingredients exist as different conformers that undergo very fast interconversion processes at human body temperature, a fact that may have implications for the effective molecular shape and thus potentially for the mechanism of action of these drugs.

Since amorphous supercooled liquid mitotane is reported to be stable in amorphous form under geometric confinement, we investigated the crystallization kinetics near room temperature both by isothermal dielectric spectroscopy measurements and optical microscopy, and found that this drug crystallized in lamellar-like domains with only sporadic nucleation during growth of the crystallites. Near room temperature, the crystallization time increases with temperature and displays a non-linear correlation with the structural relaxation time. Comparison with other glass formers shows that such non-linear correlation can only have qualitative validity in general, while it cannot be used for quantitative predictions. These results further indicate that bulk mitotane cannot be maintained in the supercooled liquid state for long times at room temperature, and therefore that it is the nanoconfinement in micellar dispersions that is responsible for the kinetic metastability of the supercooled liquid phase of recently reported mitotane formulations. This entails that, in order to achieve a better dissolution profile exploiting the amorphous form of the drug, either confinement in a porous carrier or dispersion in a polymer matrix are likely to be suitable methods to achieve kinetically stable formulations of this drug, a line of research that is worth pursuing to enhance the bioavailability of mitotane. It will be extremely interesting to investigate, for example, up to what size of the supercooled liquid mitotane domains these could be kinetically stable, if heteromolecular interactions with the surfactant moieties play a role, and whether encapsulation in a gel matrix is

sufficient to metastabilize amorphous mitotane domains.

Declaration of Competing Interest

The authors declare that they have no known competing financial interests or personal relationships that could have appeared to influence the work reported in this paper.

Data availability

Data will be made available on request.

Acknowledgments

This research was funded by the Spanish Ministry of Economy and Competitiveness MINECO through project PID2020-112975 GB-I00, and by the Generalitat de Catalunya (Catalonia, Spain) under the project 2017SGR-42.

References

Alvarez, F., Alegría, A., et al., 1991. Relationship between the time-domain Kohlrausch-Williams-Watts and frequency-domain Havriliak-Negami relaxation functions. Phys. Rev. B 44, 7306–7312.
Alvarez, F., Alegría, A., et al., 1993. Interconnection between frequency-domain Havriliak-Negami and time-domain Kohlrausch-Williams-Watts relaxation functions. Phys. Rev. B 47, 125–130.
Angell, C.A., 1985. Spectroscopy Simulation and Scattering, and the Medium Range Order Problem in Glass. J. Non-Cryst. Solids 73, 1–17.
Angell, C.A., 1988. Structural instability and relaxation in liquid and glassy phases near the fragile liquid limit. J. Non-Cryst. Solids 102, 205–221.
Arora, S.K., Bates, R.B., 1976. Crystal structure of 1-(o-chlorophenyl)-1-(p-chlorophenyl)-2,2-dichloroethane. J. Org. Chem. 41 (3), 554–556.
Attivi, D., Ajana, I., et al., 2010. Development of microemulsion of mitotane for improvement of oral bioavailability. Drug Development and Industrial Pharmacy 36 (4), 421–427.
Attivi, D. (2010) Mise en forme et amélioration de la biodisponibilité d'un anticancéreux destiné à la voie orale: exemple du mitotane. PhD thesis.
Avrami, M., 1939. Kinetics of Phase Change. I General Theory. *J. Chem. Phys.* 7, 1103–1112.
Avrami, M., 1940. Kinetics of Phase Change. II transformation – time relations for random distribution of nuclei. J. Chem. Phys. 8, 212–224.
Barrio, M., Espeau, P., et al., 2009. Polymorphism of progesterone: relative stabilities of the orthorhombic phases I and II inferred from topological and experimental pressure-temperature phase diagrams. J. Pharm. Sci. 98, 1657–1670.
Battung, F., Hassan, E., Sansoe, L., 2013. Self-microemulsifying mitotane composition. US8486445B2.
Bhardwaj, S., Arora, K., et al., 2013. Correlation between molecular mobility and physical stability of amorphous itraconazole. Mol. Pharmaceutics 10, 694–700.
Biggar, J.W., Riggs, R.L., 1974. Apparent solubility of organochlorine insecticides in water at various temperatures. Hilgardia 42 (10), 383–391.
Böhmer, R., Ngai, K.L., et al., 1993. Nonexponential relaxations in strong and fragile glass formers. J. Chem. Phys. 99, 4201–4209.
Bradley, J.-C., Williams, A., et al., 2014. Jean-Claude Bradley Open Melting Point Dataset. *figshare*. Dataset. https://doi.org/10.6084/m9.figshare.1031637.v2.
Caporaletti, F., Capaccioli, S., et al., 2019. A microscopic look at the Johari-Goldstein relaxation in a hydro-gen-bonded glass-former. Sci. Rep. 9, 14319.
Cole, R.H., Cole, K.S., 1942. Dispersion and Absorption in Dielectrics II. Direct Current Characteristics. *J. Chem. Phys.* 10, 98.
Craig, D., Royall, P., et al., 1999. The relevance of the amorphous state to pharmaceutical dosage forms: glassy drugs and freeze-dried systems. Int. J. Pharm. 179, 179–207.
Crossley, J., Smyth, C.P., 1969. Microwave absorption and molecular structure in liquids. LXXIII. A dielectric study of solute-solvent interactions. J. Am. Chem. Soc. 91, 10, 2482–2487.
Cueto, C., Brown, J.H., 1958. The chemical fractionation of an adrenocorticolytic drug. Endocrinology 62, 326–333.
D'Amore, A., Kenny, J.M., et al., 1990. Dynamic-mechanical and dielectric characterization of PEEK crystallization. Polym. Eng. Sci. 30 (5), 314–320.
Fang, V.S., 1979. Cytotoxic activity of 1-(o-chlorophenyl)-1-(pchlorophenyl)-2,2-dichloroethane (mitotane) and its analogs on feminizing adrenal neoplastic cells in culture. Cancer Res. 39, 139–145.
Gupta, P., Chawla, G., et al., 2004. Physical stability and solubility advantage from amorphous celecoxib: the role of thermodynamic quantities and molecular mobility. Mol. Pharmaceutics 1, 406–413.
Haider, M.S., Schreiner, J., et al., 2020. A micellar mitotane formulation with high drug-loading and solubility: physico-chemical characterization and cytotoxicity studies in 2D and 3D In Vitro Tumor Models. Macromol. Biosci. 20 (1), 1900178.
Haider, M.S., Ahmad, T., et al., 2021. The Challenging Pharmacokinetics of Mitotane: An Old Drug in Need of New Packaging. Eur. J. Drug Metab. Pharmacokinet. 46, 575–593.
Hassan, E., 2015. Self micro-emulsifying drug delivery system with increased bioavailability. WO2012071043A1.
Havriliak, S., Negami, S.A., 1967. Complex Plane Representation of Dielectric and Mechanical Relaxation Processes in Some Polymers. Polymer 8, 161–210.
Hellwig, H., Nowok, A., et al., 2020. Conformational analysis and molecular dynamics of glass-forming aromatic thiacrown ethers. Phys. Chem. Chem. Phys. 22, 17948–17959.
Hutter, A.M., Kayhoe, D.E., 1966. Adrenal cortical carcinoma. Results of treatment with o, p'-DDD in patients. Am. J. Med. 41 (4), 581–592.
Kissi, E.O., Grohganz, H., et al., 2018. Glass-Transition Temperature of the β-Relaxation as the major predictive parameter for recrystallization of neat amorphous drugs. J. Phys. Chem. B 122 (10), 2803–2808.
Madan, M.P., 1975. Microwave Absorption and Dielectric Relaxation of 1,2-Dihaloge-noethanes in Dilute Solutions. J. Chem. Soc., Faraday Trans. 2, 71, 67–70.
Mascia, L., Kouparitsas, Y., et al., 2020. Antiplasticization of Polymer Materials: structural aspects and effects on mechanical and diffusion-controlled properties. Polymers 12, 769.
Mehta, M., Ragoonanan, V., et al., 2016. Correlation between molecular mobility and physical stability in pharmaceutical glasses. Mol. Pharmaceutics 13 (4), 1267–1277.
Moolenaar, A.J., van Slooten, H., et al., 1981. Blood levels of o, p'-ddd following administration in various vehicles after a single dose and during long-term treatment. Cancer Chemother. Pharmacol. 7 (1), 51–54.
Moy, R.H., 1961. Studies of the pharmacology of o, p'-DDD in man. J. Lab. Clin. Med. 58, 296–304.
Musial, S.P., Freeman, C.J., et al., 1985. Mitotane (o, p′-DDD) emulsion and tablet analysis by high-performance líquid chromatography. J. Chromatogr. 319, 467–470.
Nelson, A.A., Woodard, G., 1949. Severe adrenal cortical atrophy (cytotoxic) and hepatic damage produced in dogs by feeding 2,2-bis(parachlorophenyl)-1,1-dichloroethane (DDD or TDE). Arch. Pathol. 48, 387–394.
Ngai, K.L., 1998. Relation between some secondary relaxations and the α relaxations in glass-forming materials according to the coupling model. J. Chem. Phys. 109, 6982.
Ngai, K.L., 2007. Why the glass transition problem remains unsolved? J. Non-Cryst. Solids 353, 709–718.
Ngai, K.L., Paluch, M., 2004. Classification of secondary relaxation in glass-formers based on dynamic properties. J. Chem. Phys. 120, 857–873.
Ngai, K.L., Lunkenheimer, P., et al., 2019. Predicting the α-relaxation time of glycerol confined in 1.16 nm pores of zeolitic imidazolate frameworks. Phys. Chem. Chem. Phys. 22, 507–511.
Ngai, K.L., Wojnarowska, Z., et al., 2020. The structural α-relaxation times of prilocaine confined in 1 nm pores of molecular sieves: quantitative explanation by the coupling model. Phys. Chem. Chem. Phys. 22 (17), 9257–9261.
Novikov, V.N., Rössler, E.A., 2013. Correlation between glass transition temperature and molecular mass in non-polymeric and polymer glass formers. Polymer 54 (26), 6987–6991.
Riggleman, R.A., Douglas, J.F., et al., 2007. Tuning polymer melt fragility with antiplasticizer additives. J. Chem. Phys. 126, 234903.
Romanini, M., Barrio, M., et al., 2017. Thermodynamic scaling of the dynamics of a strongly hydrogen-bonded glass-former. Sci. Rep. 7, 1346.
Romanini, M., Lorente, M., et al., 2018. Enhancement of the physical and chemical stability of amorphous drug-polymer mixtures via cryogenic comilling. Macromolecules 51 (22), 9382–9392.
Romanini, M., Rodriguez, S., et al., 2019. Nose temperature and anticorrelation between recrystallization kinetics and molecular relaxation dynamics in amorphous morniflumate at high pressure. Mol. Pharmaceutics 16, 3514–3523.
Romanini, M., Macovez, R., et al., 2021. Inter-enantiomer conversion dynamics and Johari-Goldstein relaxation of benzophenones. Sci. Rep. 11, 20248.
Ruiz, G.N., Romanini, M., et al., 2017. Relaxation Dynamics vs Crystallization Kinetics in the Amorphous State: the Case of Stiripentol. Mol. Pharmaceutics 14 (11), 3636–3643.
Ruiz, G.N., Combarro-Palacios, I., et al., 2019. Tuning molecular dynamics by hydration and confinement: antiplasticizing effect of water in hydrated prilocaine nanoclusters. Phys. Chem. Chem. Phys. 21 (28), 15576–15583.
Takano, R., Furumoto, K., et al., 2008. Rate-limiting steps of oral absorption for poorly water-soluble drugs in dogs; prediction from a miniscale dissolution test and a physiologically-based computer simulation. Pharm. Res. 25 (10), 2334–2344.
Tanaka, H., 2005. Relationship among glass-forming ability, fragility, and short-range bond ordering of liquids. J. Non-Cryst. Solids 351, 678–690.
Temple Jr., T.E., Jones Jr., D.J., et al., 1969. Treatment of Cushing's disease: Correction of hypercortisolism by o, p'-DDD without induction of aldosterone deficiency. N. Engl. J. Med. 281, 801–805.
Terzolo, M.; Baudin, A. E.; et al.. (2013) Mitotane levels predict the outcome of patients with adrenocortical carcinoma treated adjuvantly following radical resection. *Eur. J. Endocrinol.* 169, 263–2706].
Tripathi, P., Romanini, M., et al., 2015. Collective relaxation dynamics and crystallization kinetics of the amorphous Biclotymol antiseptic. Int. J. Pharmaceutics 495 (1), 420–427.
Trotta, M., Gallarate, M., et al., 2001. Emulsions containing partially water-miscible solvents for the preparation of drug nanosuspensions. J. Control. Release 76 (1-2), 119–128.
Valenti, S., Diaz, A., et al., 2019. Amorphous binary dispersions of chloramphenicol in enantiomeric pure and racemic poly-lactic acid: morphology, molecular relaxations, and controlled drug release. Int. J. Pharmaceutics 568, 118565.
Valenti, S., Barrio, M., et al., 2021. Correction to "comparative physical study of three pharmaceutically active benzodiazepine derivatives: crystalline versus amorphous state and crystallization tendency". Mol. Pharmaceutics 18, 3926–3927.

Waszut, U., Szyskza, P., et al., 2017. Understanding mitotane mode of action. J. Physiol. Pharmacol. 68, 13–26.
Watson, A.D., Rijnberk, A., et al., 1987. Systemic availability of o, p'-ddd in normal dogs, fasted and fed, and in dogs with hyperadrenocorticism. Res. Vet. Sci. 43, 160–165.
Wunderlich, B. (1976) Macromolecular Physics. Crystal Nucleation, Growth, Annealing, Vol. 2. Academic Press, London.
Yousefzade, O., Valenti, S., et al., 2019. Segmental Relaxation and Partial Crystallization of Chain-Extended Poly(L-Lactic Acid) Reinforced with Carboxylated Carbon Nanotube. *J. Polym. Sci.* Part B: Polym. Phys. 57, 222–233.
Zhou, D., Zhang, G., et al., 2002. Physical stability of amorphous pharmaceuticals: Importance of configurational thermodynamic quantities and molecular mobility. J. Pharm. Sci. 91, 1863–1872.